Relationships between photosynthesis and formaldehyde as a probe of isoprene emission

Y. Zheng[1], N. Unger[1,2], M. P. Barkley[3], and X. Yue[2]

[1]Department of Geology and Geophysics, Yale University, New Haven, Connecticut 06511, USA
[2]School of Forestry and Environmental Studies, Yale University, New Haven, Connecticut 06511, USA
[3]EOS group, Department of Physics and Astronomy, University of Leicester, Leicester, UK

Correspondence to: Y. Zheng (yiqi.zheng@yale.edu)

Abstract. Atmospheric oxidation of isoprene emission from land plants affects radiative forcing of global climate change. There is an urgent need to understand the factors that control isoprene emission variability on large spatiotemporal scales but such direct observations of isoprene emission do not exist. Two readily available global-scale long-term observation-based data sets hold information about surface isoprene activity: gross primary productivity (GPP) and tropospheric formaldehyde column variability (HCHOv). We analyze multi-year seasonal linear correlations between observed GPP and HCHOv. The observed GPP–HCHOv correlation patterns are used to evaluate a global Earth system model that embeds three alternative leaf-level isoprene emission algorithms. GPP and HCHOv are decoupled in the summertime in the southeast US ($r = -0.03$). In the Amazon, GPP and HCHOv are weakly correlated in March-April-May (MAM), correlated in June-July-August (JJA) and weakly anticorrelated in September-October-November (SON). Isoprene emission algorithms that include soil moisture dependence demonstrate greater skill in reproducing the observed interannual seasonal GPP–HCHOv correlations in the southeast US and the Amazon. In isoprene emission models that include soil moisture dependence, isoprene emission is correlated with photosynthesis and anticorrelated with HCHOv. In an isoprene emission model without soil moisture dependence, isoprene emission is anticorrelated with photosynthesis and correlated with HCHOv. Long-term monitoring of isoprene emission, soil moisture and meteorology is required in water-limited ecosystems to improve understanding of the factors controlling isoprene emission and its representation in global Earth system models.

1 Introduction

Isoprene emission, a by-product of photosynthesis, is fundamental in global chemistry–climate interactions. The global annual source strength is estimated at 0.5 Pg C year^{-1} (Guenther et al., 2006), which is of comparable magnitude to the present day total (anthropogenic and biogenic) annual source of methane (CH_4) (Kirschke et al., 2013), and the net carbon dioxide (CO_2) emission from land use change (Ciais et al., 2013). Isoprene emission rate depends upon ecosystem type, photosynthesis, temperature, and atmospheric CO_2, and is therefore sensitive to changes in land cover and climate (Monson et al., 2007). In contrast to CH_4 and CO_2, isoprene is highly reactive in the atmosphere with a lifetime of around only half an hour in the boundary layer. The atmospheric photo-oxidation of isoprene regulates the global budgets and variability of the major short-lived climate pollutants: tropospheric ozone (O_3), CH_4 and secondary organic aerosol (Arneth et al., 2010; Carslaw et al., 2010). Large-scale perturbations to isoprene emission influence global climate change (Scott et al., 2014; Unger, 2014a). In Earth's history, plant isoprene emission is recognized as an important terrestrial biogeochemical feedback that influences the global climate sensitivity (Beerling et al., 2007, 2011; Unger and Yue, 2014). Emerging research begins to quantify isoprene's role as an anthropogenic climate forcing mechanism (Heald and Spracklen, 2015; Unger, 2014b). While short-term (hours to days) weather-related fluctuations in isoprene emission in the temperate zone are well understood (Guenther et al., 1995, 1991), many open questions remain as to the long-term (months to years) factors controlling isoprene

emission. A complete understanding of isoprene emission on large spatiotemporal scales is imperative to allow for reliable projections of future air quality and global climate change, and to discern quantitatively the real-world effectiveness of mitigation strategies involving the short-lived climate pollutants.

Two readily available global observation-based data sets do hold information about isoprene emission variability: (i) gross primary productivity (GPP) and (ii) satellite tropospheric formaldehyde (HCHO) columns. GPP is the total amount of CO_2 removed from the atmosphere by plant photosynthesis. Isotopic labeling studies have shown that 70–90 % of isoprene production is directly linked to photosynthesis that provides energy and precursors for isoprene biosynthesis in the chloroplast (Affek and Yakir, 2003; Delwiche and Sharkey, 1993; Karl et al., 2002). Precipitation controls photosynthesis in more than 40 % of vegetated land (Beer et al., 2010). HCHO is a high-yield product of isoprene oxidation and has a lifetime of only a few hours against photolysis and oxidation by the hydroxyl radical (OH) during the day. Other HCHO sources include oxidation from CH_4, which provides a slowly varying background of HCHO, oxidation from other volatile organic compounds (VOCs), and direct emission from fires. Precipitation might affect HCHO indirectly by removing reactive carbon, nitrogen oxides and oxidants, thus dampening atmospheric photochemistry. Since isoprene emission frequently dominates the nonmethane VOC budget over continental land, HCHO columns have been used as a direct proxy for inferring isoprene emissions (Barkley et al., 2008, 2013; Fu et al., 2007; Millet et al., 2008; Palmer et al., 2003, 2006).

Neither GPP nor HCHO columns offer a perfect indicator of isoprene emission variability. In the case of GPP, incomplete coupling between isoprene emission and photosynthesis occurs due to the different temperature optimums of the processes, response to short-term drought and elevated atmospheric CO_2, and onset time in the deciduous biome (Harrison et al., 2013). The optimal temperature for photosynthesis is around 25 °C while isoprene emission has a higher thermal optimum of 35–40 °C. In the case of HCHO columns, limitations in use as a direct proxy for isoprene include (1) uncertainties associated with the HCHO vertical column retrieval (Barkley et al., 2012; Hewson et al., 2013), (2) distinguishing the component of the HCHO column produced solely from isoprene oxidation, and (3) uncertainties in isoprene oxidation chemistry.

Isoprene provides an intrinsic linkage between GPP and atmospheric HCHO. A recent study found a strong intraseasonal correlation between satellite HCHO columns and canopy temperature but a weak correlation or even anticorrelation with GPP in 22 regions selected to minimize interference from fires (Foster et al., 2014). In that study, HCHO columns were assumed to be a direct proxy for surface isoprene emission. Soil moisture availability was not explicitly considered as a driving variable even though water availability and canopy temperature are tightly coupled through stomatal conductance and the canopy energy balance. Accounting for soil moisture dependence of isoprene emission decreases the global source strength by 25–30 % (Müller et al., 2008; Unger et al., 2013).

Here, we investigate the multi-year (2005–2011) seasonal relationships between global observational data sets of FLUXNET-derived GPP and fire-screened satellite HCHO columns as a probe of isoprene emission on longer seasonal to interannual temporal scales. We assume that observed GPP and HCHO columns hold quantitative information about isoprene emission variability, but we do not assume that either is a direct proxy. The study proceeds in three steps. First, we calculate the covariance of the observation-based GPP and satellite HCHO columns with key meteorological variables. Then, we compute the linear correlation between GPP and HCHO observations. Finally, we use the observed GPP–HCHO relationships to evaluate a global Earth system model that incorporates three alternative isoprene emission algorithms. The models are used to interpret the observed GPP–HCHO relationships. We focus our discussion on the major isoprene emitting source regions: the southeastern US (31–35° N, −94 to −79° E) and the Amazon (−15° S to 3° N, −76 to −54° E).

2 Methods

2.1 Observational and reanalysis data sets

In this study we apply data sets of observation-derived GPP, satellite-based tropospheric HCHO columns and meteorology reanalysis. The monthly mean global GPP data set is generated using data-orientated diagnostic upscaling of site-level-derived GPP from FLUXNET (Beer et al., 2010; Bonan et al., 2011; Jung et al., 2011) and is available for years 1982–2011 with native resolution of 0.5° × 0.5° latitude by longitude. The main steps of the upscaling procedure are processing FLUXNET observational data and calculating GPP for each site, training model-tree ensembles (MTEs) for each GPP using site-level explanatory variables, and applying the established MTEs using global gridded data set of the same explanatory variables to obtain the global GPP estimates (Jung et al., 2011). A total of 29 explanatory variables are used to train the MTE, including the fraction of absorbed photosynthetically active radiation (fAPAR), precipitation, temperature and other climate and land cover data (Jung et al., 2011). The uncertainties are mainly from but not limited to (1) measurement of eddy covariance fluxes (Lasslop et al., 2008; Richardson et al., 2006), (2) the choice of explanatory variables (Jung et al., 2011), (3) gap filling and extrapolation to different environmental domains and temporal periods (Jung et al., 2009), and (4) global gridded explanatory variables (Hicke, 2005; Zhao et al., 2006). The derived GPP in tropical and subtropical regions is less well constrained

with observations and has larger uncertainties compared to the midlatitudes (Beer et al., 2010; Jung et al., 2011).

The fire-screened monthly mean tropospheric HCHO vertical columns are retrieved by the Ozone Monitoring Instrument (OMI) over 2005–2013. We compute the fire-screened tropospheric HCHO vertical columns from retrieved slant columns provided in the official NASA OMI product (González Abad et al., 2015), in a three-step process. First, we apply our own reference sector correction to normalize the HCHO columns, on a daily basis. This is a standard technique used in many studies to remove retrieval biases (e.g., Barkley et al., 2013; González Abad et al., 2015; Marais et al., 2012). Here we compute the median OMI slant columns (Ω_{SM}) in $1°$ latitude bins over the remote Pacific Ocean (140–160° W) and subtract this latitudinal bias from all retrieved slant columns (Ω_S). We then renormalize the vertical columns (Ω_V) by adding a model HCHO latitudinal background (Ω_{VB}), provided by the NASA ModelE2-YIBs simulation (described in Sect. 2.2), as follows:

$$\Omega_V = \frac{\Omega_S - \Omega_{SM}}{AMF} + \Omega_{VB}, \qquad (1)$$

where AMF is the air mass factor, defined as the ratio of the slant and vertical columns. Second, we generate AMF lookup tables using monthly averaged HCHO profiles from the global Earth system model NASA ModelE2-YIBs (three subversions, as described in Sect. 2.2), appropriate to the OMI's overpass time. The AMF calculation is the same as that described in Barkley et al. (2013), with the exception that no aerosol correction is applied as model aerosol optical depth (AOD) profiles were not available. Third, we then apply the AMFs to the corrected slant columns, using Eq. (1), and average the resulting vertical columns onto a generic global $0.5° \times 0.5°$ latitude–longitude grid. We additionally filter the OMI data, excluding scenes with $\geq 40\%$ cloud cover and that do not meet standard quality checks (González Abad et al., 2015); observations affected by the documented OMI row anomaly are also discarded. To remove biomass burning contamination from the data, we adopt the method devised by Barkley et al. (2013) which excludes fire-affected scenes using Advanced Along-Track Scanning Radiometer (AATSR) and Moderate Resolution Imaging Spectroradiometer (MODIS) active burning detections. Individual observations are discarded if a fire occurs in the $0.5°$ grid cell in which it falls or those immediately adjacent (within ± 2 grid cells) of both the current or preceding day. The uncertainties on the gridded OMI vertical columns – mainly due to cloud contamination, the a priori-modeled isoprene emissions, and the HCHO vertical column retrieval – are estimated at 5–20 % (Barkley et al, 2013). To ensure consistency in our satellite–model comparisons, the reference correction and AMFs are recomputed using HCHO profiles from the appropriate model simulation. In our subsequent analysis, we use the HCHO column variability (HCHOv), which is defined as the anomaly between local and zonal mean of the gridded fire-screened HCHO tropospheric column concentrations for each month, to explore its climatic covariance and relationship with GPP and compare against the NASA ModelE2-YIBs output. There are two main limitations in using HCHOv as a proxy for isoprene emission: (1) HCHO from CH_4 oxidation is not strictly zonally uniform, so HCHOv does not purely represent the influence of the non-methane VOCs; and (2) HCHOv is dominated by isoprene emission but their relationship is smeared by other VOCs such as biogenic terpenes and anthropogenic VOCs.

We use monthly mean meteorological variables, including surface skin temperature (T_s), downward shortwave radiation (SW), photosynthetically active radiation (PAR), and precipitation (P), from the NASA Modern Era Retrospective-Analysis for Research and Applications (MERRA) (Rienecker et al., 2011). The spatial resolution of the MERRA data is $0.5° \times 0.667°$ latitude by longitude and the temporal availability is 1979–present.

All of the monthly average observational data sets are linearly interpolated to $2.0° \times 2.5°$ latitude by longitude spatial resolution.

2.2 Global Earth system model (NASA ModelE2-YIBs)

This study applies the NASA GISS (Goddard Institute for Space Studies) ModelE2 global chemistry–climate model at $2° \times 2.5°$ latitude by longitude horizontal resolution with 40 vertical layers extending to 0.1 hPa (Schmidt et al., 2014). The Yale Interactive Terrestrial Biosphere model (YIBs) is embedded inside NASA ModelE2 in a framework known as NASA ModelE2-YIBs. The global climate model provides the meteorological drivers for the vegetation biophysics. The land-surface hydrology submodel provides soil characteristics to the vegetation physiology in each grid cell. The model framework fully integrates the land biosphere–oxidant–aerosol system such that these components interact with each other and with the physics of the climate model at the 30 min integration time step. The atmospheric composition model has been well tested against observations and compared with other models (e.g., Koch et al., 2009; Myhre et al., 2013; Shindell et al., 2013a, b; Stevenson et al., 2013).

The vegetation is described using eight plant functional types (PFTs): tundra, C3 and C4 grasslands, shrub, deciduous, tropical rainforest, evergreen, and crop. Present-day vegetation cover fractions are derived from MODIS satellite data as used in the Community Land Model and converted to the eight PFTs here (Lawrence and Chase, 2007). Gridded spatially varying PFT-specific leaf area index (LAI) is derived from Advanced Very High Resolution Radiometer (AVHRR) satellite data and linearly interpolated into daily values (Lawrence and Chase, 2007).

The canopy biophysical fluxes are computed using the well-established Farquhar leaf model of photosynthesis (von Caemmerer and Farquhar, 1981; Farquhar et al., 1980) and the stomatal conductance model of Ball and Berry (Ball et

al., 1987). The model vertically stratifies each canopy into an adaptive number of layers (typically 2–16) that distinguish LAI profiles for sunlit and shaded leaves (Friend and Kiang, 2005).

2.2.1 Isoprene emission algorithms

NASA ModelE2-YIBs incorporates two conceptually different leaf-level isoprene emission algorithms that are embedded within the exact same host simulation framework: (1) Y-PS: isoprene emission is calculated as a function of electron transport-limited photosynthesis, intercellular and atmospheric CO_2 and canopy temperature (Unger et al., 2013); and (2) Y-MEGAN: isoprene emission is calculated using empirical functions of canopy temperature and light commonly applied in The Model of Emissions of Gases and Aerosols from Nature (MEGAN) (Guenther et al., 1995). MEGAN is the most widely used system for estimating isoprene emissions from terrestrial ecosystems (Guenther et al., 2012). We test a third isoprene emission algorithm identical to Y-MEGAN but with an additional empirical multiplier to account for soil moisture availability (Y-MEGAN-SM).

In Y-PS, leaf-level isoprene emission is modeled as follows:

$$I_{emis} = \varepsilon \times J_e \times \delta \times \tau, \tag{2}$$

where ε is the PFT-specific isoprene emission potential in units of fraction of electrons available for isoprene synthesis. J_e is the electron-transport-limited photosynthesis rate (in units of $\mu mol\,m^{-2}[leaf]\,s^{-1}$). J_e is a linear function of the incident photosynthetically active radiation (PAR) and the internal leaf CO_2 concentration (C_i):

$$J_e = a_{leaf} \times PAR \times \alpha_{qe} \times \frac{C_i - \Gamma^*}{C_i + 2\Gamma^*}, \tag{3}$$

where a_{leaf} is the leaf-specific light absorptance, α_{qe} is the intrinsic quantum efficiency for photosynthetic CO_2 uptake in photosystem II (a product of the fraction of absorbed light that reaches photosystem II and the CO_2 per absorbed photon), and Γ^* is the CO_2 concentration compensation point in the absence of non-photorespiratory respiration (Collatz et al., 1991).

The δ term in Eq. (2) translates the electron flux into isoprene equivalents given by Eq. (4) (detailed in Niinemets et al., 1999; Pacifico et al., 2011):

$$\delta = \frac{C_i - \Gamma^*}{6(4.67C_i + 9.33\Gamma^*)}. \tag{4}$$

The temperature relationship (τ) in the algorithm accounts for the difference in temperature optimum between photosynthesis and isoprene synthase:

$$\tau = \exp[0.1(T - T_{ref})], \tag{5}$$

where T is leaf temperature (in °C) and T_{ref} is the leaf temperature under standard conditions (30 °C).

In Y-MEGAN, leaf-level isoprene emission is modeled as follows:

$$I_{emis} = E \times C_T \times C_L, \tag{6}$$

where E is the PFT-specific isoprene emission potential (in units of $\mu mol\,C\,m^{-2}\,s^{-1}$). C_T and C_L are defined as follows:

$$C_T = \frac{\exp\frac{C_{T1}(T_K - T_{Ks})}{RT_{Ks}T_K}}{1 + \exp\frac{C_{T2}(T_K - T_M)}{RT_{Ks}T_K}}, \tag{7}$$

$$C_L = \frac{\alpha C_{L1} PAR}{\sqrt{1 + \alpha^2 (PAR)^2}}. \tag{8}$$

T_K is the leaf temperature (in K), T_{Ks} is the leaf temperature at standard conditions (303 K), R is the ideal gas constant (8.314 $J\,K^{-1}\,mol^{-1}$) and C_{T1} (95 000 $J\,mol^{-1}$), C_{T2} (230 000 $J\,mol^{-1}$), T_M (314 K), α (0.0027) and C_{L1} (1.066) are empirical coefficients.

Y-PS and Y-MEGAN use identical PFT-specific isoprene emission potentials converted to the relevant units for ε (unitless) and E ($\mu mol\,C\,m^{-2}\,s^{-1}$), presented here in units of micrograms of carbon per gram per hour ($\mu g\,C\,g^{-1}\,h^{-1}$): tundra = 0, C3 grassland = 16, C4 grassland = 0, shrub = 16, deciduous = 45, tropical rainforest = 24, evergreen = 8, and crop = 0 (Guenther et al., 2006; Lathiere et al., 2006). An additional multiplier to account for the long-term atmospheric CO_2 sensitivity of isoprene emission is applied to both isoprene models and is normalized to 1.0 for the present-day atmospheric CO_2 levels used in this study (Arneth et al., 2007).

Y-MEGAN-SM is identical to Y-MEGAN but includes an additional multiplier to account for soil moisture availability following the approach used in the coupled photosynthesis–stomatal conductance vegetation biophysics submodel. The multiplier value is between 0 and 1 and reflects the relationship between soil water amount and the extent of stomatal closure ranging from no water stress to the soil moisture stress onset point (s^*) through to the wilting point (s_{wilt}) (Porporato et al., 2001). The multiplier value is reduced linearly between the PFT-specific values of s^* and s_{wilt} based on the climate model's soil water volumetric saturation in six soil layers. Values of s^* and s_{wilt} are documented in Unger et al. (2013).

The leaf-level isoprene emissions in each isoprene scheme are upscaled to the canopy level using the YIBs canopy vertical stratification and integration scheme (Unger et al., 2013). The canopy level isoprene fluxes are passed to the model's atmosphere through the land-surface scheme on the 30 min integration time step of the global climate model. Thus, the three isoprene emission algorithms "see" the exact same PFT-specific isoprene emission potentials (basal rates), vegetation input data and meteorology, and apply the exact same upscaling from leaf to canopy. In Y-PS, the light dependence occurs through the linkage to photosynthesis; in Y-MEGAN

and Y-MEGAN-SM, isoprene emission is directly related to PAR. All three models are directly linked to canopy temperature. In Y-PS, soil moisture dependence occurs through the linkage to photosynthesis; Y-MEGAN has no direct soil moisture dependence but captures indirect effects through canopy temperature changes; and Y-MEGAN-SM has soil moisture dependence through the additional empirical multiplier.

2.2.2 Simulations

We perform three NASA ModelE2-YIBs simulations representative of present-day (2000s) climatology for each of the isoprene emission schemes (Y-PS, Y-MEGAN, Y-MEGAN-SM). Decadal average (1996–2005) monthly varying sea surface temperature and sea ice climatology from the HadSST2 (Hadley Centre sea surface temperature) data set provide the physical climatic boundary conditions for the simulations (Rayner et al., 2006). The present-day anthropogenic trace gas and aerosol emissions are prescribed to year 2000 values from the inventory developed for IPCC AR5 (Lamarque et al., 2010). Atmospheric levels of long-lived greenhouse gases are prescribed as $CO_2 = 370$ ppmv, $CH_4 = 1733$ ppbv in the Southern Hemisphere (SH) and 1814 ppbv in the Northern Hemisphere (NH), and $N_2O = 316$ ppbv. Integrations of 11 model years are completed for all control and sensitivity simulations; the first 2 years of the simulations are discarded as spin-up and the remaining 9 years are used for analyses.

3 Results

The goal of this work is to investigate the large-scale observationally derived climatic covariance and correlations in the photosynthesis–HCHO system, and to assess the models' ability to reproduce these observationally derived biosphere–atmosphere system sensitivities and to expose the implications for isoprene emission. Therefore, instead of direct comparison between simulated and observed GPP and HCHO columns, we conduct a multiple linear regression (MLR) analysis in Sect. 3.1 and a correlation analysis in Sect. 3.2, and use the observed climatic covariance and correlations to evaluate the NASA ModelE2-YIBs model embedded with three isoprene algorithms. The direct comparison results are included in the Supplement for reference: simulated and FLUXNET-derived GPP are of comparable absolute amounts (Fig. S1 in the Supplement), while simulated tropospheric HCHO columns are considerably higher than those obtained from the OMI retrieval by about a factor of 2 (Fig. S2), which is likely due to the large uncertainties in the models as well as the satellite retrieval. In the following analysis, we apply a minimum threshold for GPP (monthly mean GPP > 0.01 g[C] m^{-2} day^{-1}) to avoid inclusion of meaningless noise, especially in boreal winter (December-January-

February) when most NH regions have very low GPP and isoprene emissions.

Using the exact same vegetation input data, meteorology and PFT-specific basal rates, the three isoprene algorithms give substantially different annual global isoprene emission strengths: 382 Tg[C] year^{-1} for Y-PS, 452 Tg[C] year^{-1} for Y-MEGAN and 263 Tg[C] year^{-1} for Y-MEGAN-SM. As shown in Fig. 1 (left column), isoprene emission in Y-MEGAN is lower in NH midlatitudes than Y-PS and is stronger in the tropics. Y-MEGAN-SM has lower isoprene flux than Y-MEGAN, especially in the dry subtropics in South America, Africa and Australia. Yet, the three OMI HCHO column data sets that use different AMFs for the three isoprene models show a similar distribution (Fig. 1, right column). Further analysis of OMI HCHO column data sets, including the MLR of HCHOv with meteorological variables in Sect. 3.1 and the observation correlation between GPP and HCHOv in Sect. 3.2, show no difference among the three HCHO data sets. Therefore, in the following analyses, results shown are based on OMI HCHO processed using Y-PS AMFs.

3.1 Meteorological drivers of GPP and HCHOv

The regionally averaged meteorological variables T_s, PAR, SW and P for the period 2005–2011 from MERRA reanalysis and the climate model NASA ModelE2-YIBs are summarized in Table 1. In MERRA, the average T_s values for March-April-May (MAM), June-July-August (JJA) and September-October-November (SON) in key regions are, respectively, (in °C) 18.0 ± 0.8, 26.8 ± 0.5, 18.6 ± 0.8 (southeast US); and 23.5 ± 0.5, 23.7 ± 0.4, 25.3 ± 0.6 (Amazon). Seasonal average T_s in the southeast US in JJA and in the Amazon in SON slightly exceed the photosynthetic thermal optimum (25 °C). No vegetated region on the planet has a seasonal average T_s that exceeds the thermal optimum of isoprene emission (35–40 °C).

We perform a multiple linear regression analysis of FLUXNET-derived GPP and OMI-retrieved HCHOv against major meteorological variables to examine their climatic covariance and to determine the most important meteorological drivers in different regions and different seasons. Figure 2 shows the MLR results for monthly mean GPP (1982–2011) and HCHOv (2005–2013) in 3 seasons (MAM, JJA, SON) against T_s, PAR (SW for HCHOv), and P. MLR of GPP and HCHOv using 2005–2011 data (the overlapped time range) yield very similar results. A provocative implication is that the effects of decadal climate change (e.g., the rapid global rise in atmospheric CO_2 since 1982) do not appear to influence GPP's and HCHOv's seasonal climatic covariance in the contemporary period. The computed standardized partial regression coefficients (β coefficients) represent the rate of change in the dependent variable for a unit change in the independent variable with all other independent variables held constant. The coefficients have been
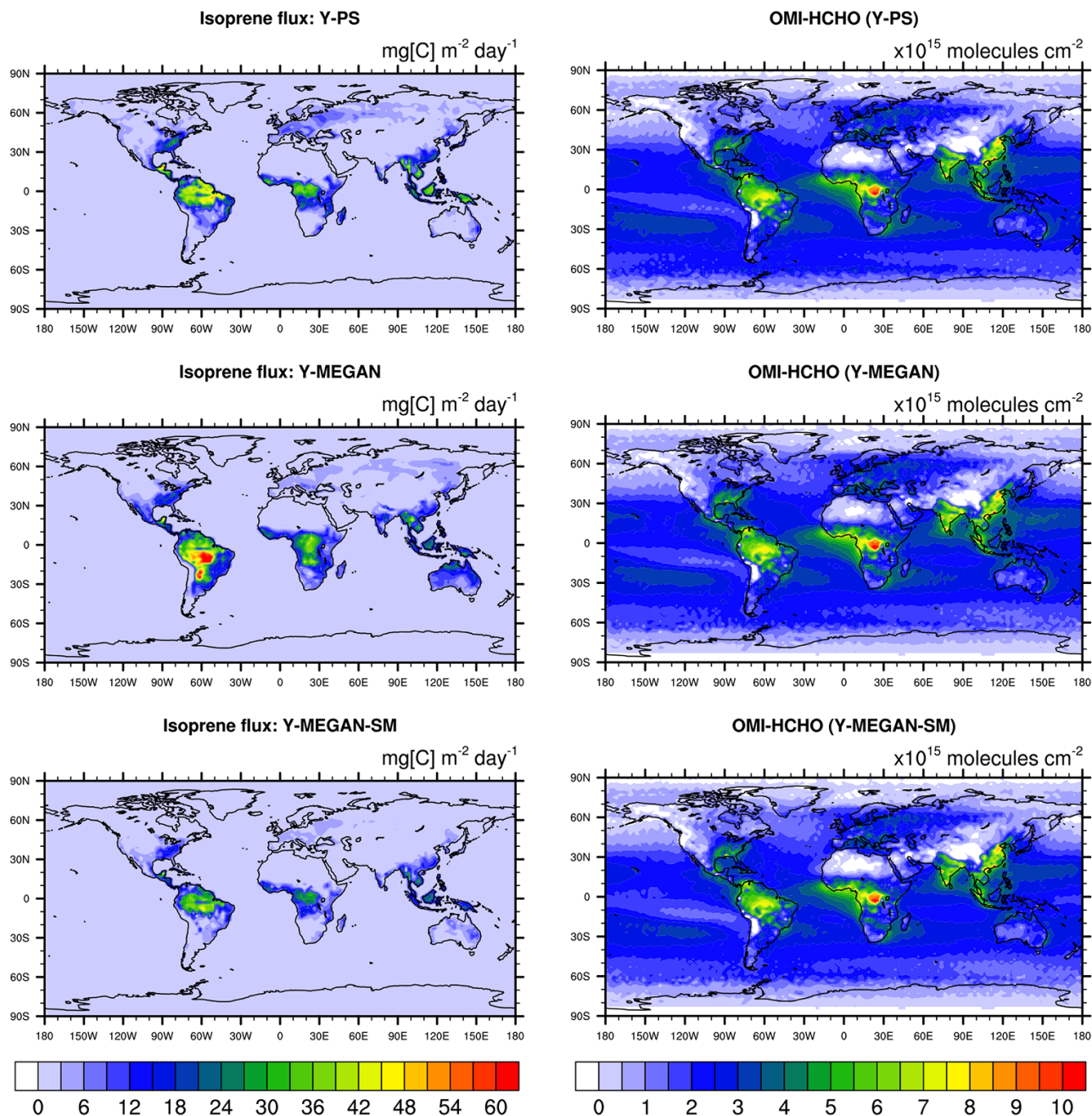
Figure 1. Left column: simulated annual mean isoprene flux (mg[C] m^{-2} day^{-1}) in models Y-PS, Y-MEGAN and Y-MEGAN-SM. Right column: satellite-based HCHO columns ($\times 10^{15}$ molecules cm^{-2}) from OMI processed using air-mass factors of models Y-PS, Y-MEGAN and Y-MEGAN-SM.

standardized in units of standard deviation; thus, they can be directly compared with each other to determine the relative importance of the different driving variables. The standardized partial regression coefficients of GPP and HCHOv associated with T_s, PAR (SW for HCHOv) and P are denoted as GPP_β_T_s, GPP_β_PAR, GPP_β_P, and HCHOv_β_T_s, HCHOv_β_SW, HCHOv_β_P. GPP β coefficients are statistically significant ($p < 0.05$) over most vegetated regions

of the planet. HCHOv β coefficients are not significant to 95 % confidence level anywhere on the planet. It is not surprising that the FLUXNET-derived GPP climatic covariance results have high statistical significance values because this product is an empirically upscaled data set based on machine learning techniques (see Sect. 2.1) using a large set of climatic and land cover explanatory variables, and the driving variables T_s, PAR and P used to determine the MLR in

Table 1. Regionally averaged meteorological variables with standard deviation from MERRA reanalysis and NASA ModelE2-YIBs in the southeast US and the Amazon.

		T_s (°C)	PAR (W m^{-2})	SW (W m^{-2})	P (mm day^{-1})
		Southeast US			
MERRA	MAM	18.0 ± 0.8	110.1 ± 3.4	250.0 ± 8.3	2.6 ± 0.7
	JJA	26.8 ± 0.5	108.5 ± 3.7	237.8 ± 9.0	4.8 ± 0.5
	SON	18.6 ± 0.8	80.7 ± 4.3	182.3 ± 10.5	2.8 ± 0.7
ModelE2-YIBs	MAM	18.6 ± 0.8	106.8 ± 2.3	237.4 ± 5.0	4.2 ± 0.5
	JJA	26.8 ± 0.4	118.7 ± 1.5	263.7 ± 3.4	4.5 ± 0.6
	SON	20.5 ± 1.3	82.1 ± 1.9	182.4 ± 4.2	2.3 ± 0.7
		Amazon			
MERRA	MAM	23.5 ± 0.5	89.9 ± 2.7	193.4 ± 6.0	7.9 ± 0.4
	JJA	23.7 ± 0.4	99.4 ± 3.1	219.9 ± 7.6	3.5 ± 0.5
	SON	25.3 ± 0.6	103.3 ± 4.2	226.0 ± 9.7	4.9 ± 0.6
ModelE2-YIBs	MAM	26.4 ± 0.2	100.3 ± 0.8	222.8 ± 1.7	6.0 ± 0.3
	JJA	26.4 ± 0.3	94.0 ± 0.9	208.9 ± 2.1	2.2 ± 0.2
	SON	28.6 ± 0.4	102.6 ± 1.0	228.1 ± 2.1	3.3 ± 0.3
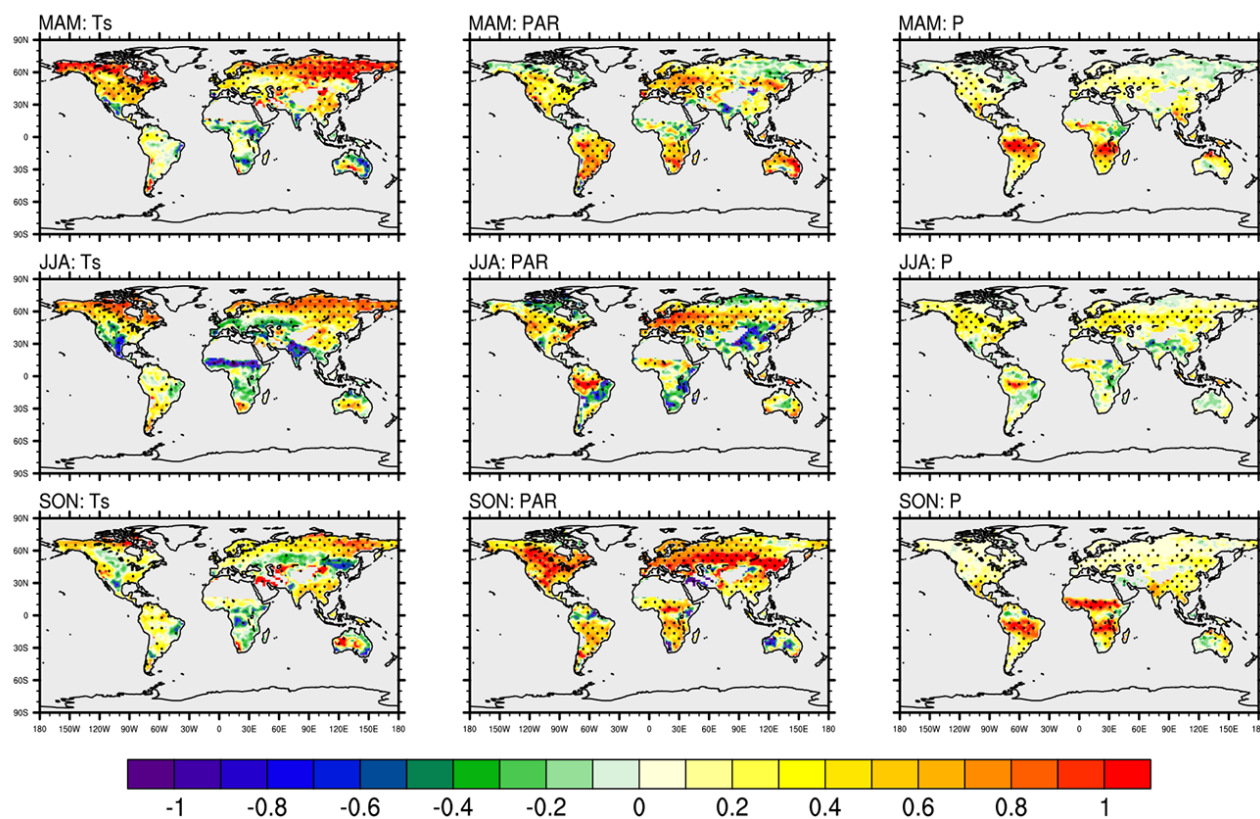
Figure 2.

(b) MLR of OMI-HCHOv 2005-2013
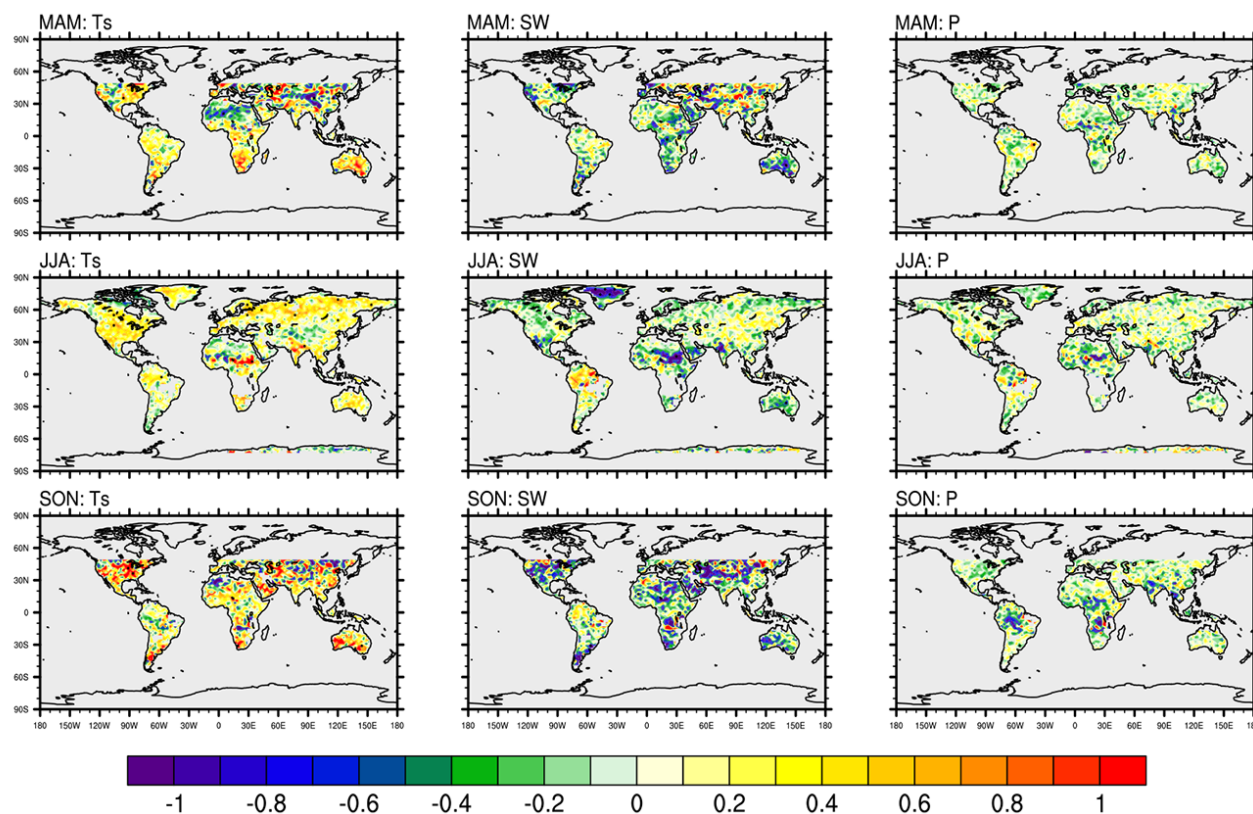
Figure 2. (a) The covariance of FLUXNET GPP with monthly mean T_s, PAR and P in MAM (top), JJA (middle) and SON (bottom) from the MLR analysis. MLR is calculated using monthly mean data in 1982–2011. Significant regions ($p < 0.05$) are shown with dotted shading. **(b)** The covariance of OMI HCHOv with monthly mean T_s, SW and P in MAM (top), JJA (middle) and SON (bottom) from the MLR analysis. MLR is calculated using monthly mean data in 2005–2013. Significant regions ($p < 0.05$) are shown with dotted shading.

this study are an important subset of the original explanatory variables. In contrast, remotely sensed HCHO columns are relatively noisy due to the satellite retrieval method (Palmer et al., 2001; De Smedt et al., 2008). Other reasons for the differences in statistical significance are that (1) satellite-based HCHO columns have many missing values due to product quality control (e.g., contamination by clouds) and the biomass burning removal (see Sect. 2.1); (2) the GPP data set has a longer record (1982–2011) than the HCHO data set (2005–2013); and (3) unlike GPP which has a simple near-parabolic relationship with T_s, HCHO dependence on T_s is more complex. For instance, increasing T_s promotes isoprene emission and oxidation to HCHO but also accelerates the chemical destruction of HCHO (see Supplement and Fig. S4).

The regionally averaged β coefficients over the southeast US (31–35° N, −94 to −79° E) and the Amazon (−15 to 3° N, −76 to −54° E) are summarized in Table 2. GPP is strongly positively related to T_s in the NH springtime and summertime at high latitudes (Fig. 2). In NH midlatitudes during the summer, where T_s values approach and/or exceed

the photosynthetic thermal optimum, sensitivity to T_s decreases dramatically. In the southeast US, GPP_β_T_s drops from 0.58 in spring to 0.03 in summer. In NH subtropical and semiarid regions there is a marked anticorrelation with T_s in the NH summer (GPP_β_$T_s < -0.3$). In contrast, HCHOv is generally positively correlated with T_s across all continents and seasons. The averaged HCHOv_β_T_s values in the southeast US are 0.36, 0.31 and 0.53 in MAM, JJA and SON. In the Amazon, the temperature dependence of both GPP and HCHOv are positive but weak.

GPP has a strong positive relationship with PAR in NH midlatitudes (especially in SON) and in tropical continents in all seasons (Fig. 2). The spatial pattern of HCHOv dependence on SW is extremely patchy because HCHO can be both formed and destroyed by photolysis. In the southeast US, GPP_β_PAR are 0.44, 0.41 and 0.51 in MAM, JJA and SON, whereas HCHOv_β_SW are, respectively, −0.02, 0.16 and −0.18; the Amazon also shows relatively strong positive light dependence of GPP (0.46, 0.57, 0.17). In the Amazon, HCHOv displays no apparent relationship with SW in MAM and SON but a positive relationship in JJA (0.00, 0.31, 0.01).

Table 2. Regionally averaged MLR β coefficients with standard deviation for GPP and HCHOv in the southeast US, defined as 31–35° N, −94 to −79° E, and the Amazon, defined as −15° S to 3° N, −76 to −54° E. The covariance of GPP with T_s, PAR and P are denoted as GPP_β_T_s, GPP_β_PAR and GPP_β_P; the covariance of HCHOv with T_s, SW and P are denoted as HCHOv_β_T_s, HCHOv_β_SW and HCHOv_β_P. In MLR of OMI HCHOv (a), (b) and (c), the OMI HCHO columns are processed using model Y-PS, Y-MEGAN and Y-MEGAN-SM, respectively.

Southeast US		
MLR of FLUXNET GPP: 1982–2011		
GPP_β_T_s	GPP_β_PAR	GPP_β_P

	GPP_β_T_s	GPP_β_PAR	GPP_β_P
MAM	0.58 ± 0.11	0.44 ± 0.10	0.19 ± 0.05
JJA	0.03 ± 0.25	0.41 ± 0.52	0.35 ± 0.30
SON	0.41 ± 0.13	0.51 ± 0.10	0.18 ± 0.08

MLR of OMI HCHOv: 2005–2013

	HCHOv_β_T_s	HCHOv_β_SW	HCHOv_β_P
MAM	(a) 0.36 ± 0.34	(a) -0.02 ± 0.32	(a) 0.05 ± 0.35
	(b) 0.36 ± 0.33	(b) -0.02 ± 0.31	(b) 0.05 ± 0.35
	(c) 0.36 ± 0.33	(c) -0.02 ± 0.31	(c) 0.04 ± 0.35
JJA	(a) 0.31 ± 0.22	(a) 0.16 ± 0.38	(a) 0.26 ± 0.51
	(b) 0.31 ± 0.22	(b) 0.17 ± 0.38	(b) 0.26 ± 0.51
	(c) 0.31 ± 0.22	(c) 0.17 ± 0.38	(c) 0.26 ± 0.51
SON	(a) 0.53 ± 0.77	(a) -0.18 ± 0.67	(a) -0.02 ± 0.37
	(b) 0.51 ± 0.77	(b) -0.16 ± 0.66	(b) -0.01 ± 0.37
	(c) 0.52 ± 0.77	(c) -0.17 ± 0.66	(c) -0.01 ± 0.37

Amazon		
MLR of FLUXNET GPP: 1982–2011		

	GPP_β_T_s	GPP_β_PAR	GPP_β_P
MAM	0.11 ± 0.17	0.46 ± 0.32	0.70 ± 0.40
JJA	0.14 ± 0.20	0.57 ± 0.54	0.27 ± 0.39
SON	0.24 ± 0.19	0.17 ± 0.50	0.50 ± 0.53

MLR of OMI HCHOv: 2005–2013

	HCHOv_β_T_s	HCHOv_β_SW	HCHOv_β_P
MAM	(a) 0.16 ± 0.27	(a) 0.00 ± 0.27	(a) -0.04 ± 0.29
	(b) 0.16 ± 0.27	(b) 0.00 ± 0.27	(b) -0.05 ± 0.29
	(c) 0.16 ± 0.27	(c) 0.00 ± 0.27	(c) -0.05 ± 0.29
JJA	(a) 0.18 ± 0.33	(a) 0.31 ± 0.54	(a) 0.03 ± 0.47
	(b) 0.18 ± 0.33	(b) 0.31 ± 0.54	(b) 0.03 ± 0.47
	(c) 0.18 ± 0.33	(c) 0.31 ± 0.53	(c) 0.03 ± 0.47
SON	(a) 0.03 ± 0.46	(a) 0.01 ± 0.52	(a) -0.31 ± 0.56
	(b) 0.04 ± 0.46	(b) 0.01 ± 0.52	(b) -0.31 ± 0.56
	(c) 0.03 ± 0.46	(c) 0.01 ± 0.52	(c) -0.31 ± 0.56

The relationship between GPP and precipitation is always positive over heavily vegetated regions. GPP_β_P values tend to be weaker than GPP_β_T_s and GPP_β_PAR values in the NH middle to high latitudes but much stronger in the tropical rainforest regions in MAM and SON. In the tropics, precipitation stimulates GPP significantly in MAM and SON (GPP_β_P = 0.70 in MAM and 0.50 in SON). In con-

trast, there is no detectable relationship between precipitation and HCHOv in this region in MAM and JJA but a strong anticorrelation in SON. Precipitation dampens local photochemistry by removing reactive carbon, nitrogen compounds and oxidants. Although wet deposition is not a major sink for HCHO due to the relatively low Henry's law coefficient, pre-

Observational GPP-HCHOv R
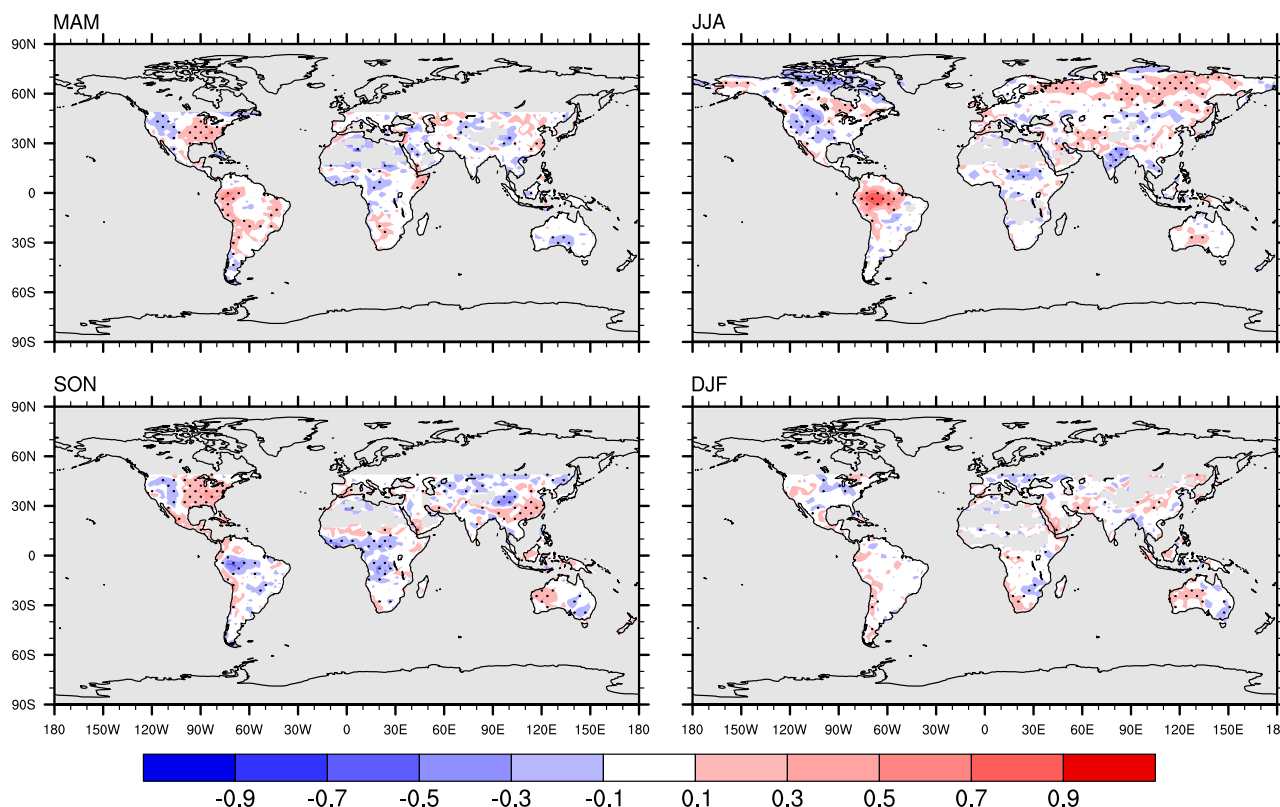
Figure 3. Observed correlation between monthly mean FLUXNET GPP and OMI HCHOv in 4 seasons: MAM, JJA, SON and DJF. Significant regions ($p < 0.05$) are shown with dotted shading.

vious studies have found an anticorrelation with precipitation in highly polluted regions (Báez et al., 1993).

3.2 Observed GPP–HCHOv correlation

Figure 3 shows the Pearson correlation coefficient (r) between monthly mean observational GPP and HCHOv for each season calculated using the 2005–2011 data. We show results where FLUXNET GPP is greater than $0.01 \, \mathrm{g[C]\, m^{-2} \, day^{-1}}$ for the latitude range $-50°$ S to $+50°$ N (except in boreal summer) because the satellite HCHO columns have known large biases in high latitudes under limited-light conditions (De Smedt et al., 2008; Wittrock et al., 2000). The observed GPP–HCHOv correlation varies strongly with latitude and season. Regionally averaged seasonal correlation values for the southeast US and the Amazon are shown in Table 3. The southeast US shows a significant GPP–HCHOv coupling in transition seasons ($r = 0.24$ in boreal spring and $r = 0.25$ in fall, $p < 0.05$), which is likely driven by their covariance with temperature. In boreal summer, this positive correlation signal moves northward to NH high latitudes where boreal forests emit terpenoids. GPP and HCHOv in the summertime in the southeast US

are almost decoupled with a very weak anticorrelation signal ($r = -0.03$). Similar decoupling or weak anticorrelation occurs in the tropics all year round except in the Amazon in JJA ($r = 0.33$).

3.3 Model GPP–HCHOv correlation

We examine the simulated GPP–HCHOv correlations in NASA ModelE2-YIBs for the three isoprene emission algorithms: Y-PS, Y-MEGAN and Y-MEGAN-SM. Overall, the simulated GPP–HCHOv r values are stronger than the observed values everywhere on the planet. Generally, over-estimates of GPP–HCHOv r values in the models may be due to oversimplified parameterizations of biogeochemical processes and photochemical oxidation mechanisms, missing possibly important but highly uncertain processes in the models, for instance nutrient availability, and the use of generic PFT-specific isoprene emission potentials. The three models successfully reproduce the GPP–HCHOv correlation pattern in the NH temperate spring and fall transition seasons that is likely driven by covariance with temperature (Fig. 4a). They broadly capture the observed GPP–HCHOv spatial patterns in the tropics in MAM and SON but not in JJA. The

Table 3. Summary of regionally averaged observational and simulated seasonal correlation coefficients in the southeast US and the Amazon. In observational GPP–HCHOv (a), (b) and (c), the OMI HCHO columns are processed using model Y-PS, Y-MEGAN and Y-MEGAN-SM, respectively.

		Southeast US		
		GPP–HCHOv	GPP–ISOPe	ISOPe–HCHOv
Observation	MAM	(a) 0.24 ± 0.10 (b) 0.24 ± 0.10 (c) 0.24 ± 0.10	–	–
	JJA	(a) -0.03 ± 0.10 (b) -0.03 ± 0.11 (c) -0.03 ± 0.10	–	–
	SON	(a) 0.25 ± 0.10 (b) 0.26 ± 0.10 (c) 0.26 ± 0.10	–	–
Y-PS	MAM	0.86 ± 0.16	0.98 ± 0.01	0.88 ± 0.14
	JJA	-0.19 ± 0.30	0.94 ± 0.07	-0.03 ± 0.31
	SON	0.68 ± 0.22	0.97 ± 0.01	0.71 ± 0.20
Y-MEGAN	MAM	0.77 ± 0.22	0.86 ± 0.14	0.97 ± 0.02
	JJA	-0.62 ± 0.19	-0.39 ± 0.23	0.73 ± 0.09
	SON	0.52 ± 0.26	0.69 ± 0.17	0.94 ± 0.05
Y-MEGAN-SM	MAM	0.81 ± 0.19	0.95 ± 0.02	0.91 ± 0.11
	JJA	-0.37 ± 0.22	0.79 ± 0.19	0.08 ± 0.35
	SON	0.61 ± 0.23	0.92 ± 0.02	0.80 ± 0.16
		Amazon		
		GPP–HCHOv	GPP–ISOPe	ISOPe–HCHOv
Observation	MAM	(a) 0.11 ± 0.19 (b) 0.11 ± 0.20 (c) 0.11 ± 0.20	–	–
	JJA	(a) 0.33 ± 0.30 (b) 0.33 ± 0.30 (c) 0.33 ± 0.30	–	–
	SON	(a) -0.09 ± 0.20 (b) -0.09 ± 0.20 (c) -0.09 ± 0.20	–	–
Y-PS	MAM	0.34 ± 0.35	0.79 ± 0.25	0.36 ± 0.31
	JJA	0.05 ± 0.46	0.84 ± 0.84	0.10 ± 0.49
	SON	-0.14 ± 0.49	0.87 ± 0.87	-0.11 ± 0.44
Y-MEGAN	MAM	0.02 ± 0.49	0.07 ± 0.54	0.31 ± 0.31
	JJA	-0.08 ± 0.51	-0.03 ± 0.62	0.62 ± 0.29
	SON	-0.51 ± 0.41	-0.46 ± 0.51	0.49 ± 0.31
Y-MEGAN-SM	MAM	0.10 ± 0.45	0.52 ± 0.42	0.14 ± 0.40
	JJA	-0.01 ± 0.49	0.45 ± 0.37	0.17 ± 0.42
	SON	-0.39 ± 0.42	0.49 ± 0.44	-0.13 ± 0.49

model's overestimate of the positive correlation in the southeast US in spring and fall may be because the algorithms do not include the delayed onset in spring or the earlier shutdown of isoprene emission before senescence. Regionally averaged model correlation results for the southeast US and the Amazon are compared with the observational results in Table 3. In contrast to the observed GPP–HCHOv decoupling (no correlation) in the summertime in the southeast US,

(a) Model GPP-HCHOv correlation
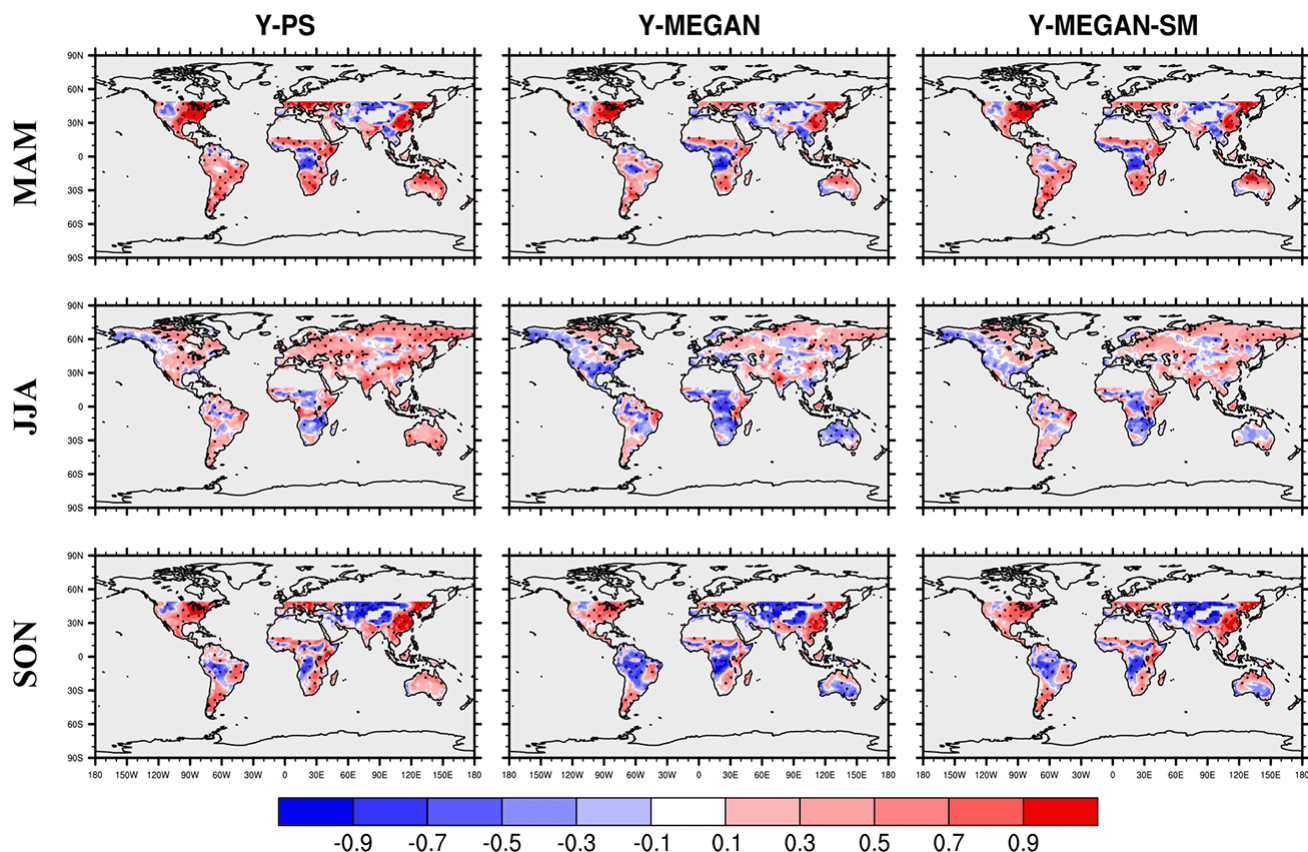
Figure 4.

the models simulate anticorrelation but to different extents: $r = -0.19$ (Y-PS), $r = -0.62$ (Y-MEGAN), $r = -0.37$ (Y-MEGAN-SM). In the Amazon, Y-PS and Y-MEGAN-SM reproduce the observed GPP–HCHOv correlations in MAM and SON but are unable to reproduce the observed strong positive correlation there in JJA. Y-MEGAN fails to reproduce the seasonal observed GPP–HCHOv correlations in the Amazon; for this model, GPP–HCHOv are anticorrelated in JJA ($r = -0.08$), where observed GPP–HCHOv $r = 0.33$, and strongly anticorrelated in SON ($r = -0.51$) where observed GPP–HCHOv $r = -0.09$. In the Amazon in JJA, GPP is strongly related to PAR; similarly, HCHOv is related to SW (Sect. 3.1).

Poor performance of all models in Amazon JJA may be due to the global climate model's simulation of meteorology. Simulated T_s ($26.4 \pm 0.3\,°C$) in the Amazon JJA is $2 \sim 3\,°C$ higher than the MERRA T_s ($23.7 \pm 0.4\,°C$) and exceeds the GPP thermal optimum ($25\,°C$). This temperature overestimation likely contributes to the non-real decoupling or weak anticorrelation between GPP and HCHOv in the three models.

To probe the underlying causes of the GPP–HCHOv relationships, we examine the model correlations between

isoprene emission (ISOPe) and GPP, and between ISOPe and HCHOv shown in Fig. 4b and c. Regionally averaged values for the southeast US and the Amazon are compared in Table 3. It is apparent that the GPP–HCHOv relationships are driven by different underlying causes contingent upon whether the isoprene emission algorithm includes soil moisture dependence. Focusing on the southeast US, Y-PS indicates linear coupling between GPP and ISOPe ($r = 0.94 \pm 0.07$), and only a weak or even anticorrelation between ISOPe and HCHOv in summertime in the southeast US ($r = -0.03 \pm 0.31$). In contrast, Y-MEGAN indicates strong coupling between ISOPe and HCHOv ($r = 0.73 \pm 0.09$), but anticorrelation between GPP and ISOPe in the summer ($r = -0.39 \pm 0.23$).

In Y-PS, anticorrelation between GPP and HCHOv is determined by the anticorrelation between ISOPe and HCHOv. On interannual seasonal timescales, precipitation positively stimulates GPP but has no direct impact on HCHOv, which is predominantly controlled by temperature (see Supplement). Precipitation may dampen photochemistry by limiting OH and O(^{1}D) concentration and thus may have an indirect impact on both formation and destruction of HCHO. Photo-

(b) Model GPP-ISOPe correlation
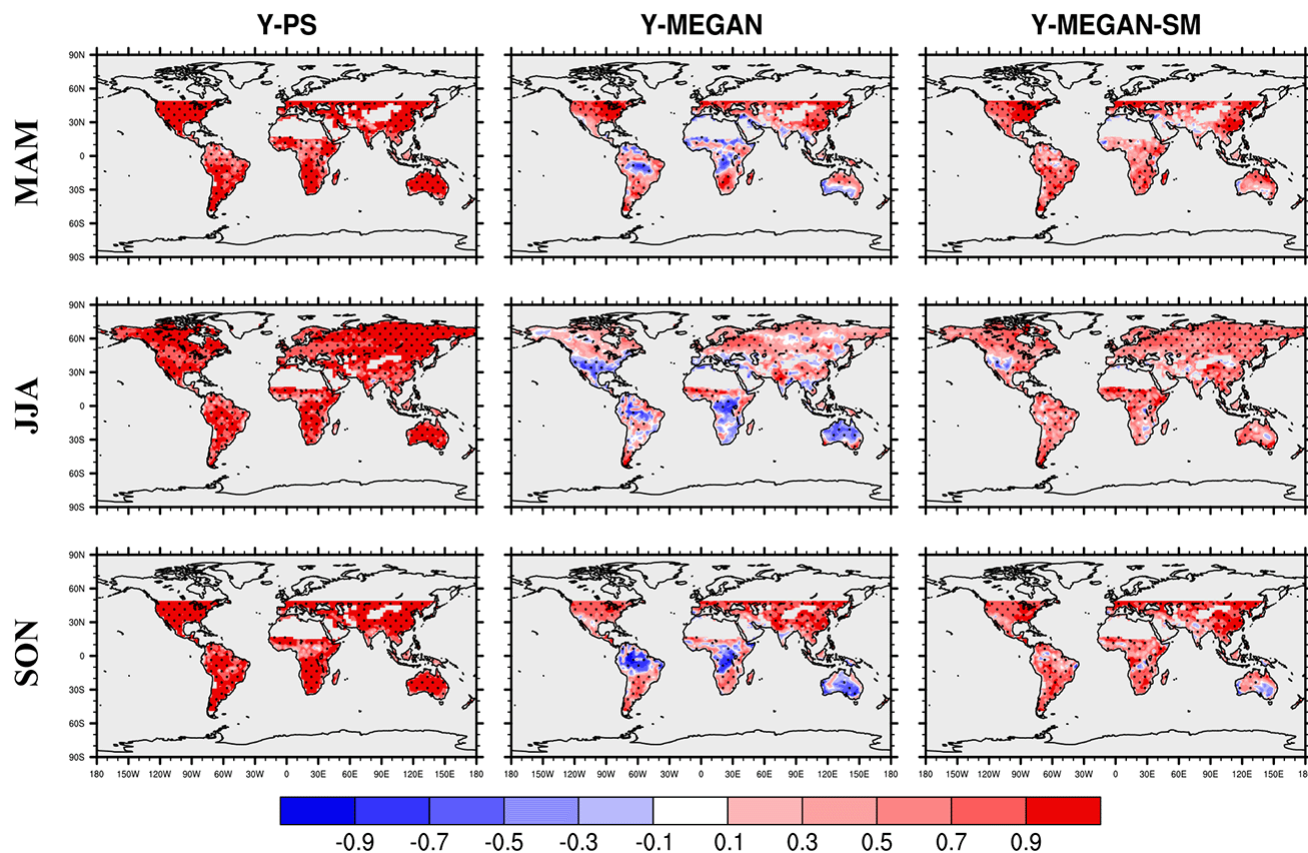
Figure 4.

chemical production and loss of HCHO strongly depend on temperature and light, independent of isoprene emission (e.g., Seinfeld and Pandis, 2006; Figs. 2b, S4). New research is showing that HCHO column variation reflects variation of OH production rather than isoprene emission variability, especially in low OH regions (L. Valin, Columbia University, personal communication, 2015). Furthermore, HCHO may be influenced by emission and oxidation of non-isoprene VOCs. In Y-MEGAN, the anticorrelation between GPP and ISOPe drives the GPP–HCHOv anticorrelation in this model under conditions when the thermal optimum of photosynthesis has been exceeded. Y-MEGAN-SM displays more Y-PS-like behavior, a correlation between GPP and ISOPe, but anticorrelation between ISOPe and HCHOv in summertime in the southeast US and in MAM and SON in the Amazon. Since the only difference between Y-MEGAN-SM and Y-MEGAN is the soil moisture dependence of isoprene emission, this result suggests the importance of water availability as a control on the photosynthesis–ISOPe–HCHO system: all the three processes are strongly influenced by temperature but the dependence on soil moisture determines the summertime covariance of photosynthesis and isoprene variabil-

ity, which can override their anticorrelation due to different thermal optima. The relative lack of sensitivity of HCHOv to water availability and precipitation leads to weaker correlation or even anticorrelation behavior between ISOPe and HCHOv.

4 Discussion and conclusions

We find that all three models reproduce the observed NH midlatitude GPP–HCHOv strong correlation in spring and fall, but predict anticorrelation in summer when the observations suggest decoupling. The underlying causes for the predicted relationships are isoprene-algorithm-dependent. In the isoprene algorithms that account for soil moisture dependence (Y-PS and Y-MEGAN-SM), interannual seasonal isoprene emission variability is tightly linked to photosynthesis but anticorrelated with HCHO variability; the dependence on soil moisture determines the summertime covariance of isoprene emission and photosynthesis, which override their opposite response to high temperature. However, in Y-MEGAN isoprene emission is anticorrelated with photosynthesis at

(c) Model ISOPe-HCHOv correlation
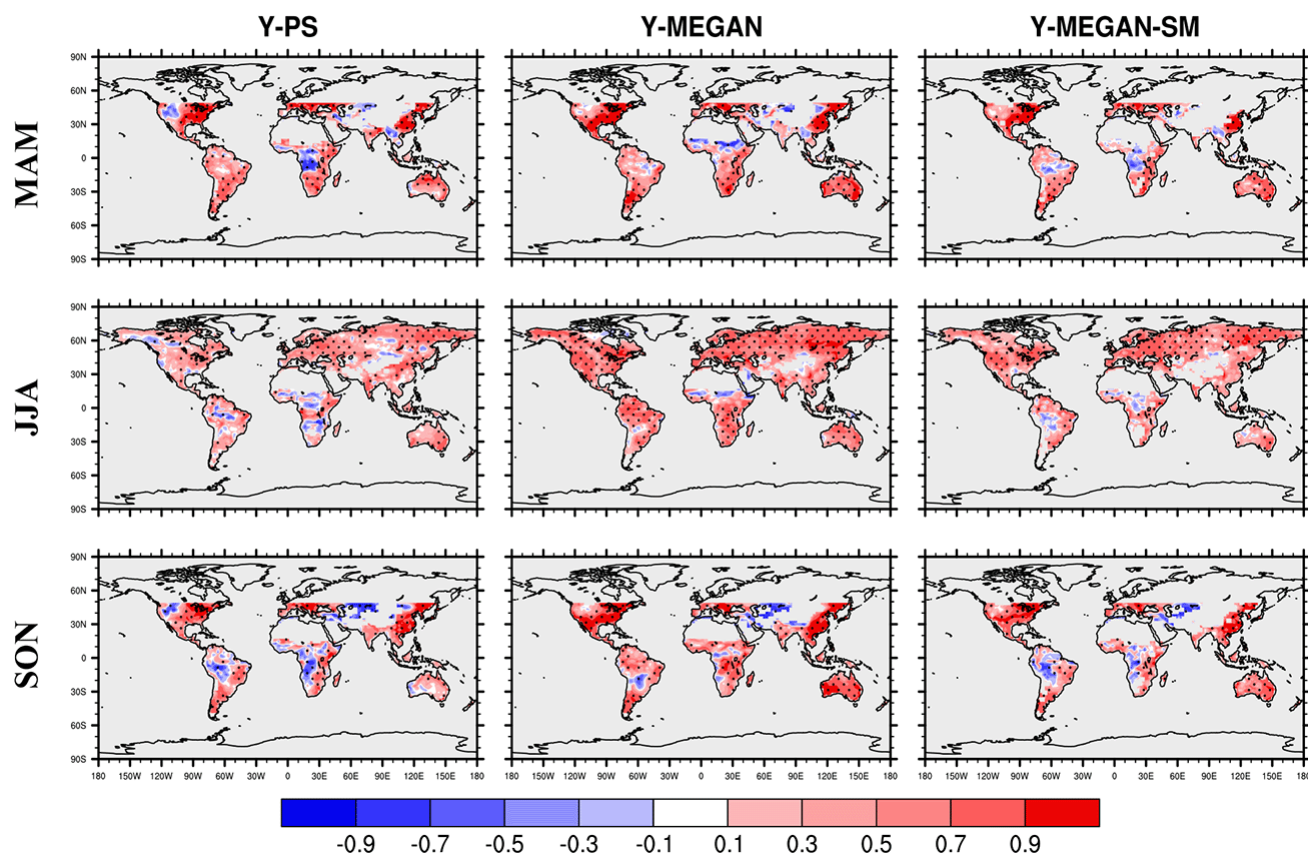
Figure 4. Simulated correlation between monthly mean **(a)** GPP and HCHOv, **(b)** GPP and ISOPe, **(c)** ISOPe and HCHOv in MAM, JJA and SON using three isoprene algorithms: Y-PS, Y-MEGAN and Y-MEGAN-SM. Significant regions ($p < 0.05$) are shown with dotted shading.

high temperatures, due to their different thermal optima, and is strongly correlated with HCHO variability. These results suggest water availability could be an important driver of isoprene emission on intraseasonal to interannual timescales.

Multiple field experiments have studied the isoprene response to water deficit conditions on different timescales. Short-time mild drought stress on a timescale of a few days affects stomatal conductance and thus the rate of photosynthesis, while does not essentially diminishing isoprene emission because photosynthetic electron transport is not inhibited (Fall and Monson, 1992; Niinemets, 2010). Several studies found increases in isoprene emission during the initial stages of mild drought conditions (e.g., Brilli et al., 2007; Pegoraro et al., 2004; Sharkey and Loreto, 1993). Severe drought or prolonged moderate drought conditions on timescales of weeks do result in significant reductions in isoprene emission that are presumably due to decreased leaf carbon availability following sustained reductions in photosynthetic rate (e.g., Brüggemann and Schnitzler, 2002; Funk et al., 2005; Sharkey and Loreto, 1993). Therefore, on the short timescales of a few days, there is a lag between isoprene

emission and photosynthetic rate in response to water stress. On longer timescales (weeks to months), isoprene emission is tightly coupled with photosynthesis, both of which are limited by soil moisture deficit. Recent studies have shown the importance of water availability on photosynthesis on interannual scales: Jung et al. (2011) suggest the interannual variability of GPP in semiarid to semihumid regions is more sensitive to precipitation rather than temperature; Beer et al. (2010) find that GPP over 40 % of the vegetated land is associated with precipitation. Therefore, despite the current lack of direct observations to constrain the soil moisture impact on the interannual variability of isoprene emission, we argue that water availability is likely to be a critical factor regulating isoprene emission on longer timescales.

This research raises more questions about long-term isoprene emission variability than it answers. Ground truthing of the findings is impeded by the lack of long-term isoprene emission flux tower and meteorology measurements in water-limited ecosystems. However, our results do suggest that water availability may be an important driver of vegetation–chemistry–climate interactions under future

global change. A corollary is that on longer timescales (seasonal, annual, decadal), GPP may be a more reliable indicator of surface isoprene emission than HCHOv. The soil moisture dependence of isoprene emission warrants further research. Long-term direct measurements of isoprene emission co-located with meteorological monitoring are essential to provide more information on the extent of water dependence of isoprene. Global Earth system models used to study long-term changes in isoprene emission should include soil moisture dependence. Currently, soil moisture is poorly represented in land-surface and climate models (Koster et al., 2009). The recent launch of the NASA Soil Moisture Active Passive instrument will produce global maps of soil moisture and is designed to help improve our understanding of the carbon and water cycles. Inadvertently, this data set may also help improve our understanding of isoprene emission and atmospheric chemistry.

Author contributions. N. Unger and Y. Zheng designed this study and developed the model code. Y. Zheng performed the simulations and analysis. M. P. Barkley processed the satellite-based formaldehyde data. X. Yue contributed to the model development. Y. Zheng, N. Unger and M. P. Barkley wrote the manuscript.

Edited by: S. Kloster

References

Affek, H. P. and Yakir, D.: Natural abundance carbon isotope composition of isoprene reflects incomplete coupling between isoprene synthesis and photosynthetic carbon flow, Plant Physiol., 131, 1727–1736, doi:10.1104/pp.102.012294, 2003.

Arneth, A., Niinemets, Ü., Pressley, S., Bäck, J., Hari, P., Karl, T., Noe, S., Prentice, I. C., Serça, D., Hickler, T., Wolf, A., and Smith, B.: Process-based estimates of terrestrial ecosystem isoprene emissions: incorporating the effects of a direct CO_2-isoprene interaction, Atmos. Chem. Phys., 7, 31–53, doi:10.5194/acp-7-31-2007, 2007.

Arneth, A., Sitch, S., Bondeau, A., Butterbach-Bahl, K., Foster, P., Gedney, N., de Noblet-Ducoudré, N., Prentice, I. C., Sanderson, M., Thonicke, K., Wania, R., and Zaehle, S.: From biota to chemistry and climate: towards a comprehensive description of trace gas exchange between the biosphere and atmosphere, Biogeosciences, 7, 121–149, doi:10.5194/bg-7-121-2010, 2010.

Báez, A. P., Padilla, H. G., and Belmont, R. D.: Scavenging of atmospheric formaldehyde by wet precipitation, Environ. Pollut., 79, 271–275, doi:10.1016/0269-7491(93)90100-3, 1993.

Ball, J. T., Woodrow, I. E., and Berry, J. A.: A Model Predicting Stomatal Conductance and its Contribution to the Control of Photosynthesis under Different Environmental Conditions, in: Progress in photosynthesis research, Springer, the Netherlands, 221–224, 1987.

Barkley, M. P., Palmer, P. I., Kuhn, U., Kesselmeier, J., Chance, K., Kurosu, T. P., Martin, R. V, Helmig, D., and Guenther, A.: Net ecosystem fluxes of isoprene over tropical South America inferred from Global Ozone Monitoring Experiment (GOME) observations of HCHO columns, J. Geophys. Res., 113, D20304, doi:10.1029/2008jd009863, 2008.

Barkley, M. P., Kurosu, T. P., Chance, K., De Smedt, I., Van Roozendael, M., Arneth, A., Hagberg, D., and Guenther, A.: Assessing sources of uncertainty in formaldehyde air mass factors over tropical South America: Implications for top-down isoprene emission estimates, J. Geophys. Res.-Atmos., 117, 1–13, doi:10.1029/2011JD016827, 2012.

Barkley, M. P., Smedt, I. De, Van Roozendael, M., Kurosu, T. P., Chance, K., Arneth, A., Hagberg, D., Guenther, A., Paulot, F., Marais, E., and Mao, J.: Top-down isoprene emissions over tropical South America inferred from SCIAMACHY and OMI formaldehyde columns, J. Geophys. Res.-Atmos., 118, 6849–6868, doi:10.1002/jgrd.50552, 2013.

Beer, C., Reichstein, M., Tomelleri, E., Ciais, P., Jung, M., Carvalhais, N., Rodenbeck, C., Arain, M. A., Baldocchi, D., Bonan, G. B., Bondeau, A., Cescatti, A., Lasslop, G., Lindroth, A., Lomas, M., Luyssaert, S., Margolis, H., Oleson, K. W., Roupsard, O., Veenendaal, E., Viovy, N., Williams, C., Woodward, F. I., and Papale, D.: Terrestrial Gross Carbon Dioxide Uptake: Global Distribution and Covariation with Climate, Science, 329, 834–838, doi:10.1126/science.1184984, 2010.

Beerling, D. J., Nicholas Hewitt, C., Pyle, J. A., and Raven, J. A.: Critical issues in trace gas biogeochemistry and global change, Philos. Trans. A. Math. Phys. Eng. Sci., 365, 1629–1642, doi:10.1098/rsta.2007.2037, 2007.

Beerling, D. J., Fox, A., Stevenson, D. S., and Valdes, P. J.: Enhanced chemistry-climate feedbacks in past greenhouse worlds, P. Natl. Acad. Sci. USA, 108, 9770–9775, doi:10.1073/Pnas.1102409108, 2011.

Bonan, G. B., Lawrence, P. J., Oleson, K. W., Levis, S., Jung, M., Reichstein, M., Lawrence, D. M., and Swenson, S. C.: Improving canopy processes in the Community Land Model version 4 (CLM4) using global flux fields empirically inferred from FLUXNET data, J. Geophys. Res., 116, G02014, doi:10.1029/2010jg001593, 2011.

Brilli, F., Barta, C., Fortunati, A., Lerdau, M., Loreto, F., and Centritto, M.: Response of isoprene emission and carbon metabolism to drought in white poplar (Populus alba) saplings, New Phytol., 175, 244–254, doi:10.1111/j.1469-8137.2007.02094.x, 2007.

Brüggemann, N. and Schnitzler, J. P.: Comparison of isoprene emission, intercellular isoprene concentration and photosynthetic performance in water-limited oak (Quercus pubescens Willd. and Quercus robur L.) saplings, Plant Biol., 4, 456–463, doi:10.1055/s-2002-34128, 2002.

Carslaw, K. S., Boucher, O., Spracklen, D. V., Mann, G. W., Rae, J. G. L., Woodward, S., and Kulmala, M.: A review of natural aerosol interactions and feedbacks within the Earth system, Atmos. Chem. Phys., 10, 1701–1737, doi:10.5194/acp-10-1701-2010, 2010.

Ciais, P., Sabine, C., Bala, G., Bopp, L., Borvkin, V., Canadell, J., Chhabra, A., DeFries, R., Galloway, J., Heimann, M., Jones, C., Le Quere, C., Myneni, R. B., Piao, S., and P, T.: Carbon and Other Biogeochemical Cycles, in: Climate Change 2013: The Physical Science Basis. Contribution of Working Group I to the Fifth Assessment Report of the Intergovernmental Panel on Climate Change, Cambridge, UK, and New York, NY, USA, 2013.

Collatz, G. J., Ball, J. T., Grivet, C., and Berry, J. A.: Physiological and Environmental-Regulation of Stomatal Conductance, Photosynthesis and Transpiration – a Model That Includes a Laminar Boundary-Layer, Agric. For. Meteorol., 54, 107–136, 1991.

Delwiche, C. F. and Sharkey, T. D.: Rapid appearance of 13C in biogenic isoprene when 13CO2 is fed to intact leaves, Plant. Cell Environ., 650, 587–591, doi:10.1111/J.1365-3040.1993.Tb00907.X, 1993.

De Smedt, I., Müller, J.-F., Stavrakou, T., van der A, R., Eskes, H., and Van Roozendael, M.: Twelve years of global observations of formaldehyde in the troposphere using GOME and SCIAMACHY sensors, Atmos. Chem. Phys., 8, 4947–4963, doi:10.5194/acp-8-4947-2008, 2008.

Fall, R. and Monson, R. K.: Isoprene emission rate and intercellular isoprene concentration as influenced by stomatal distribution and conductance, Plant Physiol., 100, 987–992, doi:10.1104/pp.100.2.987, 1992.

Farquhar, G. D., Caemmerer, S. V., and Berry, J. A.: A Biochemical-Model of Photosynthetic Co2 Assimilation in Leaves of C-3 Species, Planta, 149, 78–90, 1980.

Foster, P. N., Prentice, I. C., Morfopoulos, C., Siddall, M., and van Weele, M.: Isoprene emissions track the seasonal cycle of canopy temperature, not primary production: evidence from remote sensing, Biogeosciences, 11, 3437–3451, doi:10.5194/bg-11-3437-2014, 2014.

Friend, A. D. and Kiang, N. Y.: Land surface model development for the GISS GCM: Effects of improved canopy physiology on simulated climate, J. Clim., 18, 2883–2902, 2005.

Fu, T.-M., Jacob, D. J., Palmer, P. I., Chance, K., Wang, Y. X., Barletta, B., Blake, D. R., Stanton, J. C., and Pilling, M. J.: Space-based formaldehyde measurements as constraints on volatile organic compound emissions in east and south Asia and implications for ozone, J. Geophys. Res., 112, D06312, doi:10.1029/2006JD007853, 2007.

Funk, J. L., Jones, C. G., Gray, D. W., Throop, H. L., Hyatt, L. A., and Lerdau, M. T.: Variation in isoprene emission from Quercus rubra: Sources, causes, and consequences for estimating fluxes, J. Geophys. Res.-Atmos., 110, 1–10, doi:10.1029/2004JD005229, 2005.

González Abad, G., Liu, X., Chance, K., Wang, H., Kurosu, T. P., and Suleiman, R.: Updated Smithsonian Astrophysical Observatory Ozone Monitoring Instrument (SAO OMI) formaldehyde retrieval, Atmos. Meas. Tech., 8, 19–32, doi:10.5194/amt-8-19-2015, 2015.

Guenther, A., Hewitt, C. N., Erickson, D., Fall, R., Geron, C., Graedel, T., Harley, P., Klinger, L., Lerdau, M., Mckay, W. A., Pierce, T., Scholes, B., Steinbrecher, R., Tallamraju, R., Tay-lor, J., and Zimmerman, P.: A Global-Model of Natural Volatile Organic-Compound Emissions, J. Geophys. Res., 100, 8873–8892, doi:10.1029/94jd02950, 1995.

Guenther, A., Karl, T., Harley, P., Wiedinmyer, C., Palmer, P. I., and Geron, C.: Estimates of global terrestrial isoprene emissions using MEGAN (Model of Emissions of Gases and Aerosols from Nature), Atmos. Chem. Phys., 6, 3181–3210, doi:10.5194/acp-6-3181-2006, 2006.

Guenther, A. B., Monson, R. K., and Fall, R.: Isoprene and monoterpene emission rate variability: Observations with eucalyptus and emission rate algorithm development, J. Geophys. Res., 96, 10799, doi:10.1029/91JD00960, 1991.

Guenther, A. B., Jiang, X., Heald, C. L., Sakulyanontvittaya, T., Duhl, T., Emmons, L. K., and Wang, X.: The Model of Emissions of Gases and Aerosols from Nature version 2.1 (MEGAN2.1): an extended and updated framework for modeling biogenic emissions, Geosci. Model Dev., 5, 1471–1492, doi:10.5194/gmd-5-1471-2012, 2012.

Harrison, S. P., Morfopoulos, C., Dani, K. G. S., Prentice, I. C., Arneth, A., Atwell, B. J., Barkley, M. P., Leishman, M. R., Loreto, F., Medlyn, B. E., Niinemets, Ü., Possell, M., Peñuelas, J., and Wright, I. J.: Volatile isoprenoid emissions from plastid to planet, New Phytol., 197, 49–57, doi:10.1111/nph.12021, 2013.

Heald, C. L. and Spracklen, D. V.: Land use change impacts on air quality and climate, Chem. Rev., 115, 4476–4496, doi:10.1021/cr500446g, 2015.

Hewson, W., Bösch, H., Barkley, M. P., and De Smedt, I.: Characterisation of GOME-2 formaldehyde retrieval sensitivity, Atmos. Meas. Tech., 6, 371–386, doi:10.5194/amt-6-371-2013, 2013.

Hicke, J. A.: NCEP and GISS solar radiation data sets available for ecosystem modeling: Description, differences, and impacts on net primary production, Global Biogeochem. Cy., 19, 1–18, doi:10.1029/2004GB002391, 2005.

Jung, M., Reichstein, M., and Bondeau, A.: Towards global empirical upscaling of FLUXNET eddy covariance observations: validation of a model tree ensemble approach using a biosphere model, Biogeosciences, 6, 2001–2013, doi:10.5194/bg-6-2001-2009, 2009.

Jung, M., Reichstein, M., Margolis, H. A., Cescatti, A., Richardson, A. D., Arain, M. A., Arneth, A., Bernhofer, C., Bonal, D., Chen, J., Gianelle, D., Gobron, N., Kiely, G., Kutsch, W., Lasslop, G., Law, B. E., Lindroth, A., Merbold, L., Montagnani, L., Moors, E. J., Papale, D., Sottocornola, M., Vaccari, F., and Williams, C.: Global patterns of land-atmosphere fluxes of carbon dioxide, latent heat, and sensible heat derived from eddy covariance, satellite, and meteorological observations, J. Geophys. Res.-Biogeo., 116, 1–16, doi:10.1029/2010JG001566, 2011.

Karl, T., Fall, R., Rosenstiel, T. N., Prazeller, P., Larsen, B., Seufert, G., and Lindinger, W.: On-line analysis of the (CO2)-C-13 labeling of leaf isoprene suggests multiple subcellular origins of isoprene precursors, Planta, 215, 894–905, doi:10.1007/S00425-002-0825-2, 2002.

Kirschke, S., Bousquet, P., Ciais, P., Saunois, M., Canadell, J. G., Dlugokencky, E. J., Bergamaschi, P., Bergmann, D., Blake, D. R., Bruhwiler, L., Cameron-Smith, P., Castaldi, S., Chevallier, F., Feng, L., Fraser, A., Heimann, M., Hodson, E. L., Houweling, S., Josse, B., Fraser, P. J., Krummel, P. B., Lamarque, J. F., Langenfelds, R. L., Le Quere, C., Naik, V., O'Doherty, S., Palmer, P. I., Pison, I., Plummer, D., Poulter, B., Prinn, R. G.,

Rigby, M., Ringeval, B., Santini, M., Schmidt, M., Shindell, D. T., Simpson, I. J., Spahni, R., Steele, L. P., Strode, S. A., Sudo, K., Szopa, S., van der Werf, G. R., Voulgarakis, A., van Weele, M., Weiss, R. F., Williams, J. E., and Zeng, G.: Three decades of global methane sources and sinks, Nat. Geosci., 6, 813–823, doi:10.1038/Ngeo1955, 2013.

Koch, D., Schulz, M., Kinne, S., McNaughton, C., Spackman, J. R., Balkanski, Y., Bauer, S., Berntsen, T., Bond, T. C., Boucher, O., Chin, M., Clarke, A., De Luca, N., Dentener, F., Diehl, T., Dubovik, O., Easter, R., Fahey, D. W., Feichter, J., Fillmore, D., Freitag, S., Ghan, S., Ginoux, P., Gong, S., Horowitz, L., Iversen, T., Kirkevåg, A., Klimont, Z., Kondo, Y., Krol, M., Liu, X., Miller, R., Montanaro, V., Moteki, N., Myhre, G., Penner, J. E., Perlwitz, J., Pitari, G., Reddy, S., Sahu, L., Sakamoto, H., Schuster, G., Schwarz, J. P., Seland, Ø., Stier, P., Takegawa, N., Takemura, T., Textor, C., van Aardenne, J. A., and Zhao, Y.: Evaluation of black carbon estimations in global aerosol models, Atmos. Chem. Phys., 9, 9001-9026, doi:10.5194/acp-9-9001-2009, 2009.

Koster, R. D., Guo, Z. C., Yang, R. Q., Dirmeyer, P. A., Mitchell, K., and Puma, M. J.: On the Nature of Soil Moisture in Land Surface Models, J. Clim., 22, 4322–4335, doi:10.1175/2009jcli2832.1, 2009.

Lamarque, J.-F., Bond, T. C., Eyring, V., Granier, C., Heil, A., Klimont, Z., Lee, D., Liousse, C., Mieville, A., Owen, B., Schultz, M. G., Shindell, D., Smith, S. J., Stehfest, E., Van Aardenne, J., Cooper, O. R., Kainuma, M., Mahowald, N., McConnell, J. R., Naik, V., Riahi, K., and van Vuuren, D. P.: Historical (1850–2000) gridded anthropogenic and biomass burning emissions of reactive gases and aerosols: methodology and application, Atmos. Chem. Phys., 10, 7017–7039, doi:10.5194/acp-10-7017-2010, 2010.

Lasslop, G., Reichstein, M., Kattge, J., and Papale, D.: Influences of observation errors in eddy flux data on inverse model parameter estimation, Biogeosciences, 5, 1311–1324, doi:10.5194/bg-5-1311-2008, 2008.

Lathière, J., Hauglustaine, D. A., Friend, A. D., De Noblet-Ducoudré, N., Viovy, N., and Folberth, G. A.: Impact of climate variability and land use changes on global biogenic volatile organic compound emissions, Atmos. Chem. Phys., 6, 2129–2146, doi:10.5194/acp-6-2129-2006, 2006.

Lawrence, P. J. and Chase, T. N.: Representing a new MODIS consistent land surface in the Community Land Model (CLM 3.0), J. Geophys. Res., 112, G01023, doi:10.1029/2006JG000168, 2007.

Marais, E. A., Jacob, D. J., Kurosu, T. P., Chance, K., Murphy, J. G., Reeves, C., Mills, G., Casadio, S., Millet, D. B., Barkley, M. P., Paulot, F., and Mao, J.: Isoprene emissions in Africa inferred from OMI observations of formaldehyde columns, Atmos. Chem. Phys., 12, 6219–6235, doi:10.5194/acp-12-6219-2012, 2012.

Millet, D. B., Jacob, D. J., Boersma, K. F., Fu, T. M., Kurosu, T. P., Chance, K., Heald, C. L., and Guenther, A.: Spatial distribution of isoprene emissions from North America derived from formaldehyde column measurements by the OMI satellite sensor, J. Geophys. Res., 113, D02307, doi:10.1029/2007jd008950, 2008.

Monson, R. K., Trahan, N., Rosenstiel, T. N., Veres, P., Moore, D., Wilkinson, M., Norby, R. J., Volder, A., Tjoelker, M. G., Briske, D. D., Karnosky, D. F., and Fall, R.: Isoprene emission from terrestrial ecosystems in response to global change: minding the gap between models and observations, Philos. Trans. R. Soc. A – Mathematical Phys. Eng. Sci., 365, 1677–1695, doi:10.1098/Rsta.2007.2038, 2007.

Müller, J.-F., Stavrakou, T., Wallens, S., De Smedt, I., Van Roozendael, M., Potosnak, M. J., Rinne, J., Munger, B., Goldstein, A., and Guenther, A. B.: Global isoprene emissions estimated using MEGAN, ECMWF analyses and a detailed canopy environment model, Atmos. Chem. Phys., 8, 1329–1341, doi:10.5194/acp-8-1329-2008, 2008.

Myhre, G., Samset, B. H., Schulz, M., Balkanski, Y., Bauer, S., Berntsen, T. K., Bian, H., Bellouin, N., Chin, M., Diehl, T., Easter, R. C., Feichter, J., Ghan, S. J., Hauglustaine, D., Iversen, T., Kinne, S., Kirkevåg, A., Lamarque, J.-F., Lin, G., Liu, X., Lund, M. T., Luo, G., Ma, X., van Noije, T., Penner, J. E., Rasch, P. J., Ruiz, A., Seland, Ø., Skeie, R. B., Stier, P., Takemura, T., Tsigaridis, K., Wang, P., Wang, Z., Xu, L., Yu, H., Yu, F., Yoon, J.-H., Zhang, K., Zhang, H., and Zhou, C.: Radiative forcing of the direct aerosol effect from AeroCom Phase II simulations, Atmos. Chem. Phys., 13, 1853–1877, doi:10.5194/acp-13-1853-2013, 2013.

Niinemets, Ü.: Mild versus severe stress and BVOCs: thresholds, priming and consequences, Trends Plant Sci., 15, 145–153, doi:10.1016/j.tplants.2009.11.008, 2010.

Niinemets, U., Tenhunen, J. D., Harley, P. C., and Steinbrecher, R.: A model of isoprene emission based on energetic requirements for isoprene synthesis and leaf photosynthetic properties for Liquidambar and Quercus, Plant Cell Environ., 22, 1319–1335, 1999.

Pacifico, F., Harrison, S. P., Jones, C. D., Arneth, A., Sitch, S., Weedon, G. P., Barkley, M. P., Palmer, P. I., Serça, D., Potosnak, M., Fu, T.-M., Goldstein, A., Bai, J., and Schurgers, G.: Evaluation of a photosynthesis-based biogenic isoprene emission scheme in JULES and simulation of isoprene emissions under present-day climate conditions, Atmos. Chem. Phys., 11, 4371–4389, doi:10.5194/acp-11-4371-2011, 2011.

Palmer, P. I., Jacob, D. J., Chance, K., Martin, R. V., Spurr, R. J. D., Kurosu, T. P., Bey, I., Yantosca, R., Fiore, A. M., and Li, Q.: Air mass factor formulation for spectroscopic measurements from satellites: Application to formaldehyde retrievals from the Global Ozone Monitoring Experiment, J. Geophys. Res., 106, 14539–14550, doi:10.1029/2003JD003652, 2001.

Palmer, P. I., Jacob, D. J., Fiore, A. M., Martin, R. V., Chance, K., and Kurosu, T. P.: Mapping Isoprene Emissions over North America using Formaldehyde Column Observations from Space, J. Geophys. Res., 108, 4180, doi:10.1029/2002JD002153, 2003.

Palmer, P. I., Abbot, D. S., Fu, T.-M., Jacob, D. J., Chance, K., Kurosu, T. P., Guenther, A., Wiedinmyer, C., Stanton, J. C., Pilling, M. J., Pressley, S. N., Lamb, B., and Sumner, A. L.: Quantifying the seasonal and interannual variability of North American isoprene emissions using satellite observations of the formaldehyde column, J. Geophys. Res., 111, D12315, doi:10.1029/2005JD006689, 2006.

Pegoraro, E., Rey, A., Greenberg, J., Harley, P., Grace, J., Malhi, Y., and Guenther, A.: Effect of drought on isoprene emission rates from leaves of Quercus virginiana Mill, Atmos. Environ., 38, 6149–6156, doi:10.1016/j.atmosenv.2004.07.028, 2004.

Porporato, A., Laio, F., Ridolfi, L., and Rodriguez-Iturbe, I.: Plants in water-controlled ecosystems: active role in hydrologic pro-

cesses and response to water stress – III. Vegetation water stress, Adv. Water Resour., 24, 725–744, doi:10.1016/S0309-1708(01)00006-9, 2001.

Rayner, N. A., Brohan, P., Parker, D. E., Folland, C. K., Kennedy, J. J., Vanicek, M., Ansell, T. J., and Tett, S. F. B.: Improved analyses of changes and uncertainties in sea surface temperature measured in situ sice the mid-nineteenth century: The HadSST2 dataset, J. Clim., 19, 446–469, 2006.

Richardson, A. D., Hollinger, D. Y., Burba, G. G., Davis, K. J., Flanagan, L. B., Katul, G. G., William Munger, J., Ricciuto, D. M., Stoy, P. C., Suyker, A. E., Verma, S. B., and Wofsy, S. C.: A multi-site analysis of random error in tower-based measurements of carbon and energy fluxes, Agric. For. Meteorol., 136, 1–18, doi:10.1016/j.agrformet.2006.01.007, 2006.

Rienecker, M. M., Suarez, M. J., Gelaro, R., Todling, R., Bacmeister, J., Liu, E., Bosilovich, M. G., Schubert, S. D., Takacs, L., Kim, G. K., Bloom, S., Chen, J. Y., Collins, D., Conaty, A., Da Silva, A., Gu, W., Joiner, J., Koster, R. D., Lucchesi, R., Molod, A., Owens, T., Pawson, S., Pegion, P., Redder, C. R., Reichle, R., Robertson, F. R., Ruddick, A. G., Sienkiewicz, M., and Woollen, J.: MERRA: NASA's Modern-Era Retrospective Analysis for Research and Applications, J. Clim., 24, 3624–3648, doi:10.1175/Jcli-D-11-00015.1, 2011.

Schmidt, G. A., Kelley, M., Nazarenko, L., Ruedy, R., Russell, G. L., Aleinov, I., Bauer, M., Bauer, S. E., Bhat, M. K., Bleck, R., Canuto, V., Chen, Y.-H., Cheng, Y., Clune, T. L., Del Genio, A., de Fainchtein, R., Faluvegi, G., Hansen, J. E., Healy, R. J., Kiang, N. Y., Koch, D., Lacis, A. A., LeGrande, A. N., Lerner, J., Lo, K. K., Matthews, E. E., Menon, S., Miller, R. L., Oinas, V., Oloso, A. O., Perlwitz, J. P., Puma, M. J., Putman, W. M., Rind, D., Romanou, A., Sato, M., Shindell, D. T., Sun, S., Syed, R. A., Tausnev, N., Tsigaridis, K., Unger, N., Voulgarakis, A., Yao, M.-S., and Zhang, J.: Configuration and assessment of the GISS ModelE2 contributions to the CMIP5 archive, J. Adv. Model. Earth Syst., 6, 141–184, doi:10.1002/2013MS000265, 2014.

Scott, C. E., Rap, A., Spracklen, D. V., Forster, P. M., Carslaw, K. S., Mann, G. W., Pringle, K. J., Kivekäs, N., Kulmala, M., Lihavainen, H., and Tunved, P.: The direct and indirect radiative effects of biogenic secondary organic aerosol, Atmos. Chem. Phys., 14, 447–470, doi:10.5194/acp-14-447-2014, 2014.

Seinfeld, J. H. and Pandis, S. N.: Atmospheric Chemistry and Physics: From Air Pollution to Climate Change, 2nd ed., Wiley, New York, USA, 2006.

Sharkey, T. D. and Loreto, F.: Water stress, temperature, and light effects on the capacity for isoprene emission and photosynthesis of kudzu leaves, Oecologia, 95, 328–333, doi:10.1007/BF00320984, 1993.

Shindell, D. T., Lamarque, J.-F., Schulz, M., Flanner, M., Jiao, C., Chin, M., Young, P. J., Lee, Y. H., Rotstayn, L., Mahowald, N., Milly, G., Faluvegi, G., Balkanski, Y., Collins, W. J., Conley, A. J., Dalsoren, S., Easter, R., Ghan, S., Horowitz, L., Liu, X., Myhre, G., Nagashima, T., Naik, V., Rumbold, S. T., Skeie, R., Sudo, K., Szopa, S., Takemura, T., Voulgarakis, A., Yoon, J.-H., and Lo, F.: Radiative forcing in the ACCMIP historical and future climate simulations, Atmos. Chem. Phys., 13, 2939–2974, doi:10.5194/acp-13-2939-2013, 2013a.

Shindell, D. T., Pechony, O., Voulgarakis, A., Faluvegi, G., Nazarenko, L., Lamarque, J.-F., Bowman, K., Milly, G., Kovari, B., Ruedy, R., and Schmidt, G. A.: Interactive ozone and methane chemistry in GISS-E2 historical and future climate simulations, Atmos. Chem. Phys., 13, 2653–2689, doi:10.5194/acp-13-2653-2013, 2013b.

Stevenson, D. S., Young, P. J., Naik, V., Lamarque, J.-F., Shindell, D. T., Voulgarakis, A., Skeie, R. B., Dalsoren, S. B., Myhre, G., Berntsen, T. K., Folberth, G. A., Rumbold, S. T., Collins, W. J., MacKenzie, I. A., Doherty, R. M., Zeng, G., van Noije, T. P. C., Strunk, A., Bergmann, D., Cameron-Smith, P., Plummer, D. A., Strode, S. A., Horowitz, L., Lee, Y. H., Szopa, S., Sudo, K., Nagashima, T., Josse, B., Cionni, I., Righi, M., Eyring, V., Conley, A., Bowman, K. W., Wild, O., and Archibald, A.: Tropospheric ozone changes, radiative forcing and attribution to emissions in the Atmospheric Chemistry and Climate Model Intercomparison Project (ACCMIP), Atmos. Chem. Phys., 13, 3063–3085, doi:10.5194/acp-13-3063-2013, 2013.

Unger, N.: Human land-use-driven reduction of forest volatiles cools global climate, Nat. Clim. Chang., 4, 907–910, doi:10.1038/nclimate2347, 2014a.

Unger, N.: On the role of plant volatiles in anthropogenic global climate change, Geophys. Res. Lett., 41, 8563–8569, doi10.1002/2014GL061616, 2014b.

Unger, N. and Yue, X.: Strong chemistry-climate feedbacks in the Pliocene, Geophys. Res. Lett., 41, 527–533, doi:10.1002/2013GL058773, 2014.

Unger, N., Harper, K., Zheng, Y., Kiang, N. Y., Aleinov, I., Arneth, A., Schurgers, G., Amelynck, C., Goldstein, A., Guenther, A., Heinesch, B., Hewitt, C. N., Karl, T., Laffineur, Q., Langford, B., A. McKinney, K., Misztal, P., Potosnak, M., Rinne, J., Pressley, S., Schoon, N., and Serça, D.: Photosynthesis-dependent isoprene emission from leaf to planet in a global carbon-chemistry-climate model, Atmos. Chem. Phys., 13, 10243–10269, doi:10.5194/acp-13-10243-2013, 2013.

Von Caemmerer, S. and Farquhar, G. D.: Some Relationships between the Biochemistry of Photosynthesis and the Gas-Exchange of Leaves, Planta, 153, 376–387, 1981.

Wittrock, F., Richter, A., Ladstätter-weißenmayer, A., and Burrows, J. P.: Global Observations of Formaldehyde, Proc. ERSEN-VISAT Symposium, ESA-Publ. SP-461, 16–20 October 2000, Gothenburg, Sweden, 2000.

Zhao, M., Running, S. W., and Nemani, R. R.: Sensitivity of Moderate Resolution Imaging Spectroradiometer (MODIS) terrestrial primary production to the accuracy of meteorological reanalyses, J. Geophys. Res.-Biogeo., 111, G01002, doi:10.1029/2004JG000004, 2006.